Dependence of slip weakening distance (D_c) on final slip during dynamic rupture of earthquakes

Elisa Tinti[(1)], Massimo Cocco[(1)], Eiichi Fukuyama[(2)] and Alessio Piatanesi[(1)]

(1) *Istituto Nazionale di Geofisica e Vulcanologia, Sezione di Sismologia e Tettonofisica, Via di Vigna Murata, 605, 00143 - Roma, ITALY.*
(tinti@ingv.it)

(2) *National Research Institute for Earth Sciences and Disaster Prevention Tsukuba, Ibaraki 305-0006, Japan.*

Summary

In this study we aim to understand the dependence of the critical slip weakening distance (D_c) on the final slip (D_{tot}) during the propagation of a dynamic rupture and the consistency of their inferred correlation. To achieve this goal we have performed a series of numerical tests suitably designed to validate the adopted numerical procedure and to verify the actual capability in measuring D_c. We have retrieved two kinematic rupture histories from spontaneous dynamic rupture models governed by a slip weakening law in which a constant D_c distribution on the fault plane as well as a constant D_c / D_{tot} ratio are assumed, respectively. The slip velocity and the shear traction time histories represent the synthetic "real" target data which we aim to reproduce. We use a 3-D traction-at-split nodes numerical procedure to image the dynamic traction evolution by assuming our modeled slip velocity as a boundary condition on the fault plane. We assume a regularized Yoffe function as source time function in our modeling attempts and we measure the critical slip weakening distance from the inferred traction versus slip curves at each point on the fault. We compare the inferred values with those of the target dynamic models. Our numerical tests show that fitting the slip velocity functions of the target models at each point on the fault plane is not enough to retrieve good traction evolution curves and to obtain reliable measures of D_c. We find that the estimation of D_c is very sensitive to any small variation of the slip velocity function. An artificial correlation between D_c/D_{tot} is obtained when a fixed shape of slip velocity is assumed on the fault (i.e., constant rise time and constant time for positive acceleration) which differs from that of the target model. We point out that the estimation of fracture energy (breakdown work) on the fault is not affected by biases in measuring D_c.

Keywords: Dynamic fault weakening, slip weakening distance, fault mechanics

1. Introduction

Several numerical approaches have been recently proposed to retrieve the evolution of dynamic traction during the earthquake propagation on extended faults. They all reveal an evident dynamic fault weakening behavior during earthquake rupture propagation, which is represented by the shear traction evolution as a function of slip. The main parameters describing this slip weakening behavior are: the initial, yield and residual (kinetic) stresses and the slip weakening distance (D_c) (see Figure 1a). The breakdown process is characterized by the shear traction degradation near the propagating crack-tip from the upper yield stress to the residual stress level. D_c characterizes the dimension of the breakdown zone and, consequently, it is associated with the duration of the breakdown process during dynamic failure.

Dynamic fault weakening is controlled by different, sometime competing, physical processes, such as thermal pressurization of pore fluid (Mase and Smith, 1987; Rice 2006; Bizzarri and Cocco 2006-a, -b), flash heating (Rice 2006; Rice and Cocco, 2007), frictional melting (Hirose and Shimamoto, 2005), production of gouge material (Matsu'ura et al., 1992) as well as formation of silica gel (Di Toro et al., 2004) due to abrasion or wear. Despite dynamic fault weakening characterizes most of traction evolution, slip hardening can often precede the beginning of the breakdown phase, although slip associated with the peak yield stress is believed to be much smaller than D_c (Ohnaka, 2003). In the following we will refer to dynamic fault weakening including both the initial slip hardening and the subsequent slip weakening phases. The aforementioned processes govern fault weakening at different length and temporal scales (Rice and Cocco, 2007; Cocco and Tinti, 2008). This implies that the constitutive laws representing each process should contain a length or a time scale parameter. A key example is represented by rate- and state-dependent constitutive laws in which the length scale parameter is L that differs from the slip weakening distance D_c inferred from traction evolution (Cocco and Bizzarri, 2002; Hillers et al., 2006). Bizzarri and Cocco (2003) have demonstrated that, in the framework of rate- and state-dependent

friction law, D_c (named d_0 by the authors) is a function of the length scale parameter *L* and the initial mechanical state.

D_c was theoretically proposed by Ida (1972) and Palmer and Rice (1973) as a key parameter of slip weakening model and was also measured by several laboratory experiments (e.g. Okubo and Dieterich, 1984; Ohnaka et al., 1987; Tsutsumi and Shimamoto, 1997; Di Toro et al., 2004; Chambon et al., 2006). D_c is one of the important input parameters for the numerical modelling of spontaneous dynamic rupture propagation (see Andrews, 1976 -a, -b; Fukuyama, 2003; Harris, 2004, among many others), because it controls the fracture energy (Abercrombie and Rice, 2005; or breakdown work, see Tinti et al., 2005a and Cocco et al., 2006). In most of numerical simulations of spontaneous dynamic rupture propagation, D_c is imposed a priori (see Mai et al., 2006 and references therein) and often is assumed to be constant and uniformly distributed on the fault plane.

The physical interpretation of D_c is still debated in the literature. Several authors proposed that both D_c and the fracture energy G are scale dependent parameters (Campillo and Ionescu, 1997; Ohnaka, 2003 and references therein). This implies that their origin and physical meaning cannot be easily inferred from seismological observations (Cocco et al., 200**9** and references therein). Ohnaka (2003) proposed that D_c is associated with the roughness of the sliding surface, which means that in this case the selected scale of macroscopic description corresponds to the thickness of the principal slipping zone (from mm to cm). Cocco and Tinti (2008) have discussed the scale dependence in the dynamics of earthquake rupture propagation by jointly interpreting and by attempting to reconcile geological and seismological measures of surface and fracture energy. Discussing the physical origin of the characteristic slip weakening distance is beyond the goals of the present study. We only emphasize that it cannot be associated with a particular physical process, without properly solving in a rigorous mathematical way the scale dependence and scale separation problem in earthquake dynamics (see Cocco and Tinti, 2008). This is of particular relevance for interpreting seismological measures of this dynamic parameter.

The value of D_c proposed in the recent literature ranges from microns as in laboratory experiments with bare surfaces (Okubo and Dieterich, 1984; Lockner and Okubo, 1983) to several meters as in laboratory experiments with gouge and high velocity frictional tests (Tsutsumi and Shimamoto, 1997; Di Toro et al., 2004, Hirose and Bystricky, 2007, among many others) or in numerical and seismological estimates (Ide and Takeo, 1997; Bouchon, 1997; Dalguer et al., 2003; Zhang et al., 2003, among many others). Numerical simulations of dynamic rupture with prescribed slip weakening laws commonly use D_c values ranging between 0.1 and ~1 m (see Fukuyama and Mikumo, 2004; Ma and Archuleta, 2006, among many others). Other numerical simulation attempts, which consider different constitutive laws that do not prescribe a priori the traction versus slip evolution (as rate and state dependent friction laws, Dieterich 1979), have also inferred D_c values in the same interval. Several physical processes induced by frictional heating, such as thermal pressurization, can modify the slip weakening curves and can affect the inferred D_c values. Simulations performed with thermal pressurization models (Andrews, 2002; Bizzarri and Cocco, 2006-a, b) also suggest that D_c ranges between 0.1 cm and several meters. In numerical simulations performed by adopting rate and state dependent friction, the parameter L is in the range of mm to cm, while D_c can range between 10 cm and 1 m. For large earthquakes (M > 6), the distribution of D_c on the fault plane is usually imaged through the reconstruction of traction time history from a kinematic slip model obtained by waveform inversions (Bouchon, 1997; Ide and Takeo, 1997; Day et al., 1998; Tinti et al. 2005a and references therein). Ide and Takeo (1997), for instance, evaluated D_c ranging between 0.5 and 1 m for the 1995 Kobe earthquake. Therefore, we can conclude that both seismological and high-velocity laboratory observations suggest estimates of D_c larger than one meter.

Pulido and Irikura (2000), Guatteri et al. (2001) and Peyrat et al. (2001), among several others, found that D_c is proportional to the final slip (D_{tot}): D_c ranges between 20% and 90% of D_{tot}. Abercrombie and Rice (2005) proposed a model in which dynamic traction evolution as a function of slip follows a power law in which D_c is equal to the slip at the last time-step increment (D_{tot}). The

correlation between D_c and D_{tot} has been reported in many other papers (Zhang et al., 2003; Tinti et al., 2005a). However, Piatanesi et al. (2004) pointed out that in the kinematic modelling the use of source time functions not compatible with the dynamic rupture propagation could bias the estimate of D_c and hence the inferred values of D_c/D_{tot}. These results raise the question of the actual size of D_c, whether it is proportional to the final slip and if it can be scaled with some other quantity such as seismic moment.

Recently, Mikumo et al. (2003) proposed a method to estimate D_c using slip velocity functions on the fault without measuring the stress behavior. The method assumes that the time of peak slip velocity and stress breakdown time are similar and therefore they estimate the slip at the time of peak slip velocity (named D_c') as an estimate of D_c. They evaluate D_c' to range between 0.4 and 0.8m (27 - 56% of D_{tot}) with an error of 20-50%. Fukuyama et al. (2003) showed that the method works well if the source model is relatively smooth. Tinti et al. (2004) confirmed that the difference between D_c' and D_c depends on the parameters of the adopted constitutive laws and can be as large as 50%. Cocco et al. (2009) present a review of the seismological estimates of D_c' and D_c from kinematic inverted source models.

Guatteri and Spudich (2000) pointed out the limitation in estimating the critical slip weakening distance by modeling ground motion waveforms due to the trade-off between D_c and strength excess. Spudich and Guatteri (2004) showed that low-pass filtering of kinematic slip models could bias inferences of D_c to large values and possibly bias fracture energy upward and radiated energy downward. The authors have also shown that low pass filtering of seismograms can affect the estimate of D_c' and can yield an artificial correlation between D_c' and D_{tot}. In addition, Yasuda et al. (2005) showed that the spatial smoothing effect also biases the estimation of D_c and concluded that the correlation between D_c' and final slip might be an artifact of limited available spatial resolution.

As mentioned before, here we will not go into the details of the origin of D_c because it is beyond the scope of this paper. Rather, we focus our attention on the main open questions concerning this

parameter: in particular, we aim to understand if the correlation between D_c and final slip D_{tot} is a real feature or it comes out from biases in retrieving traction evolution curves. Moreover, we aim to comprehend if D_c can be a large fraction of total slip (70 - 90%) and to constrain its actual size. Answering these questions will also be of relevance for not considering as reliable dynamic models with constant D_c and for elaborating spontaneous dynamic models with a constant distribution of D_c/D_{tot} on the fault plane. We will not discuss here the limitations in imaging the final slip D_{tot}, due to inadequate resolution and narrow frequency bandwidth that affect inversion approaches. However, we have to remark that poor spatial and temporal resolution will bias the estimation of D_c and D_c/D_{tot} for real earthquakes.

In the present study we use synthetic simulations to test the accuracy in retrieving the D_c distribution and its scaling with final slip. We use rupture histories modelled through spontaneous dynamic simulations as target models. We fit the slip velocity function of these target models and we use them as boundary conditions on the fault plane to infer traction evolutions (see Tinti et al. 2005a for detailed description of the methodology). We use the regularized Yoffe function proposed by Tinti et al. (2005b) to match the slip velocity functions of the target models to infer kinematic source models consistent with the dynamic propagation of an earthquake rupture (see Figure 1b) and to estimate the D_c values under a virtual condition that can not be achieved in the reality: the knowledge of "target" dynamic model. This allows us to check the real capability to infer D_c and to retrieve dynamic models with constant D_c and its scaling with D_{tot}.

2. Simulation strategy

We first compute two forward spontaneous dynamic models that we consider as "*target models*". In other words, we use these dynamic models to obtain known slip velocity and traction time histories that we will use to validate our numerical calculations. These dynamic models have the same fault geometry of a real seismic event: the 2000 western Tottori (M_w 6.6), Japan, earthquake. The dynamic forward modeling has been performed by selecting appropriate combinations of input

parameters which yield a final slip distribution on the fault plane similar to that obtained by

Mikumo et al. (2003). These authors retrieved their model by inverting the seismic waveforms

recorded during this earthquake. Despite we have computed spontaneous dynamic models which

resemble the rupture history of a real earthquake, we point out that our models have a better

resolution than those proposed by Mikumo et al. (2003). This is necessary for the goals and the

simulation strategy followed in this study. The similarity with the Tottori earthquake is not relevant

for the present study. We emphasize that we are not interested in getting insights on the physics of

this particular real earthquake, because we focus here on the issue of the reliable determination of

D_c parameter in a controlled kinematic framework. As we will discuss in the following, these two

target models differ for the distribution of the slip-weakening distance (D_c, see Figure 1a) parameter.

We therefore produce a suite of kinematic rupture models by adopting different source time

functions characterizing the slip velocity evolution, but keeping the same rupture time distribution

resulting from the spontaneous dynamic simulations and maintaining a slip distribution similar to

the original one. In other words, the different kinematic rupture models mostly differ for the

adopted source time function.

We use two different source time functions. The first one is a smoothed version of the original

slip velocity function resulting from the spontaneous dynamic models. We can consider this slip

velocity function as the optimal representation of the rupture history. It will be used for the

validation test described in section 3. The second one is obtained by fitting the true slip velocity

time history at each point on the fault plane through an inversion procedure with a regularized

Yoffe function (Piatanesi et al., 2004; Tinti et al., 2005b); this will be discussed in section 2.2.

Although other candidate source time functions are available in the literature (see for instance

Nakamura and Miyatake, 2000; Dreger et al., 2007), we adopt the Yoffe function (see Figure 1b)

because it is dynamically consistent (Nielsen and Madariaga, 2000) and because of its feasible

parameterization (see Tinti et al., 2005b) to our goals. We can consider this second slip velocity

function as the most favourable representation of the rupture history through an analytical source

time function. In this way we have derived different kinematic source models having precisely the same rupture time and similar final slip and rise time distributions, but slightly different shapes of the slip velocity functions.

In order to infer the dynamic traction evolution, we compute the spatio-temporal stress changes from each kinematic model using the slip velocity history as a boundary condition of the elastodynamic equation on the fault plane. To this goal we use the traction-at-split-node finite difference method (FDM) proposed by Andrews (1999) and implemented by Tinti et al. (2005a). Finally, through the inferred traction evolution curves we measure the dynamic parameters (dynamic stress drop, D_c, breakdown work, see Figure 1a) at each point on the fault and we map their distributions on the fault plane. The whole simulation strategy is summarized in the flow chart shown in Figure 2.

In practical applications the rupture history is imaged by inverting ground motion waveforms and geodetic data. The inverse numerical approaches either assume an analytical source time function (single window approach) or represent the source time function as the superposition of several triangular functions (multi window approach). The latter case has the advantage to avoiding the choice of the source time function but the limitation of a sparse sampling of the slip velocity time history (i.e., which means a poor resolution). The present study provides an ideal situation that would never happen for real applications to earthquakes, because in reality we cannot measure the goodness of our fit to the real (unknown) slip velocity function. Nevertheless, these synthetic tests relying on the complete knowledge of the rupture history are appropriately designed to verify our capability to infer the slip weakening distance (D_c) from earthquake kinematic models estimated from observed seismograms.

In the next subsections we discuss the simulation strategy summarized above in greater detail, providing more information on the theoretical background and the numerical procedures, including the values of main physical parameters adopted in the different steps depicted in the flow chart of Figure 2.

2.1 Spontaneous dynamic models

We employ the target model constructed by Fukuyama and Mikumo (2004), who computed the stress drop distribution from the slip distribution by solving the elasto-static equation (Fukuyama and Madariaga, 1995). Then they computed dynamic rupture propagation using the boundary integral equation method (BIEM, Fukuyama and Madariaga, 1998) assuming the slip weakening law as constitutive relation.

The dynamic parameters that have to be assumed a priori are D_c and S; the latter is defined (Das and Aki, 1977) as the ratio of strength excess (σ_y-σ_o) and stress drop (σ_o-σ_r) (see Figure 1a). Fukuyama and Mikumo (2004) computed two models: a model with constant D_c (= 0.3 m) on the fault plane (*Model 2*) and a second model with constant D_c/D_{tot} (= 0.3) and heterogeneous D_c on the fault plane (*Model 3*). Both models have the same heterogeneous distribution of stress drop corresponding to the heterogeneous distribution of final slip (Mikumo et al., 2003). Figure 3 shows the slip and stress drop distributions on the fault plane for both models.

The spatial discretization and the time step of these dynamic models are 200m and 0.01s, respectively. The fault dimension is 25.6 km along strike by 12.8 km along dip. The rupture velocity of both models is not so heterogeneous and the average value is nearly the same, about 2.7 km/s, because the same S value (= 0.3) was used in the forward dynamic modelling. The initial stress and the yield stress are non-uniformly distributed on the fault plane, while the kinetic frictional level is homogeneous. The rupture time distributions of both models are shown in Figure 4-a and b, respectively. The dynamic models have been computed in a homogeneous unbounded elastic medium, where P- and S- wave velocities and density are assumed to be 6.0 km/s, 3.55 km/s, and 2400 kg/m^3, respectively.

The heterogeneity of the stress drop and strength excess yields healing of slip and consequently both rupture models are characterized by a propagating slip pulse. This means that the local duration of slip velocity (rise time) is shorter than the total rupture duration, and heterogeneously

distributed on the fault plane. The stress and slip velocity time histories for both models in three selected target points on the fault plane (indicated in Figure 3 with open circles) are shown in Figure 5. These slip velocity functions are those resulting from the spontaneous dynamic calculations after smoothing through a Butterworth filter.

2.2. Fitting slip velocity function with Yoffe function

We build our kinematic models using the analytical source time function (STF) proposed by Tinti et al. (2005b). This STF is not singular both at the rupture onset and at the healing time. The regularized Yoffe function is characterized by three parameters: T_{acc}, τ_R^{eff} and D_{tot} (see Figure 1b). T_{acc} is the duration of the positive slip acceleration phase, τ_R^{eff} is the local duration of slip velocity (the rise time) and D_{tot} is the final slip. All these parameters are assumed independent of each other and can vary on the fault. More analytical details concerning this function can be found in Tinti et al. (2005b). The peak slip velocity (V_{peak}) is also an important parameter. It is not an independent parameter and it is related to the other three kinematic parameters through the following asymptotic relation (see Tinti et al., 2005b for details):

$$V_{peak} \approx C \frac{D_{\max}}{\sqrt{T_{acc}(\tau_R^{eff} - 1.57 T_{acc})}} \qquad (1).$$

Because T_{acc} can be heterogeneous on the fault plane, the initial slope of the slip velocity can vary among different target points on the fault. This variability of the acceleration phase along the fault is an important feature of heterogeneous rupture models obtained through spontaneous dynamic simulations. Figure 1a shows an example of traction change versus slip plot inferred at a specific target point for a model characterized by a slip pulse represented by a regularized Yoffe function propagating on the fault plane at constant rupture velocity.

In order to infer the best kinematic rupture model for stress changes calculations, we find the best values of T_{acc}, τ_R^{eff} and D_{tot} that provide an acceptable fit of the original target source time

functions at each position on the fault plane through an inversion procedure. We use a misfit

function that is a hybrid representation between L1 and L2 norms (Sen and Stoffa, 1991):

$$E = 1 - \frac{2\sum(v_0(t)v_s(t))}{\sum v_0^2(t) + \sum v_s^2(t)}$$ (2)

where $v_o(t)$ is the original slip velocity function to be fitted and $v_s(t)$ is the synthetic one. This cost

function is sensitive to both the shape and the amplitude of slip velocity time functions and it is

more robust than the standard least squares approaches.

We perform two distinct inversion attempts. In the first one, instead of inverting all three

parameters simultaneously, we have inverted only two of them (τ_R^{eff} and D_{tot}) and we have fixed

T_{acc} to be equal to the value of the target slip velocity function. This model will provide the best

resolution of slip velocities during the breakdown phase (that is the time window characterized by

dynamic fault weakening, see Figure 1c), because T_{acc} is precisely the same of the original target

model. It is important to point out that the two target models used in this study are spatially very

heterogeneous (both stress drop and strength excess are strongly non-uniform on the fault plane)

and the associated slip velocity functions of the target models are quite complex at particular

positions (for instance, between two large slip patches, the slip velocity function has two peaks).

The second inversion attempt is performed by inverting all the three parameters, T_{acc}, τ_R^{eff} and D_{tot}.

In this case, T_{acc} is not fixed and it is obtained by the inversion procedure. For both the cases, the

inversion is done for each slip velocity history of all 8192 subfaults of the fault plane.

The inversion procedure seeks for the best analytical solution that fits the target slip velocity

time history on each point on the fault plane. Because the target rupture model is quite

heterogeneous, the target slip velocity time functions can slightly differ between distinct points on

the fault surface, even for those located nearby. Despite this temporal variability of slip velocity

evolution, the spatial distribution of slip velocity of the target model on the fault plane is relatively

smooth. The kinematic models retrieved by inverting the slip velocity time histories through the

regularized Yoffe function exhibit a smoother temporal evolution than the target dynamic models,

but a more heterogeneous spatial distribution on the fault. This can be explained considering that we perform the inversion in time domain and each point of the fault plane is inverted independently of the neighbouring. Moreover, the spontaneous dynamic (target) model does not have any constrain in time: that is, the slip velocity is not imposed analytically a priori but it can evolve in time driven by stress change evolution. This means that the best fit to the target slip velocity function in time does not constrain its spatial gradient. As we will discuss in the following, this has a strong effect on the inferred traction evolution.

For this reason, we decided to invert only one out of five subsequent subfaults and we retrieve the slip velocity in the remaining positions by a spatial bicubic interpolation of the three parameters T_{acc}, τ_R^{eff} and D_{tot}. This operation represents a sort of smoothness constraint and allows us to better control the spatial gradient of slip. Because of the original target models have a high spatial resolution *(Δx = 0.2 km)*, this smoothing filter reduces the resolution to Δx = 1.0 km, that corresponds to the usual available resolution of kinematic source models.

2.3. Computation of stress time history

We use a 3-D finite difference split-node dynamic code to calculate the stress time history on the earthquake fault plane (Andrews, 1999). The stress change is computed through the fundamental elastodynamic equation (Miyatake, 1992; Ide and Takeo, 1997). The total dynamic traction in each fault position is calculated by the sum of two contributions: the instantaneous term depending on the slip velocity at the same position and the dynamic load related to the previous slip history. The explicit dependence has been found analytically by Fukuyama and Madariaga (1998). Their inferred equation is the following:

$$\sigma(\mathbf{x},t) = -\frac{\mu}{2\beta}v(\mathbf{x},t) + \int_{\Sigma}\int_0^t K(\mathbf{x}-\xi;t-t')v(\xi,t)dt'\,dS \qquad (3)$$

where $v(x, t)$ represents the slip velocity, β the shear wave velocity, μ the rigidity, K the dynamic load associated to those points that are still slipping.

In the present study, we impose the slip velocity as a boundary condition. In other words, each node belonging to the fault plane is forced to move with a prescribed slip velocity time history. In this way we do not need to specify any constitutive relation between total dynamic traction and friction and the dynamic traction evolution is a result of the calculations. The initial stress is an unknown parameter; in our calculations it is assumed constant everywhere on the fault plane, differently from the original target models. This does not affect the calculations of dynamic traction evolution because we measure only stress changes and we know that in these tests slip direction does not change with time (that is, traction and slip velocity are always collinear). The knowledge of traction evolution and slip time history allows the computation of D_c as well as all the other dynamic fundamental parameters at each grid point on the fault plane.

3. Validation test

In order to test the proposed methodology, we compare the target stress time histories resulting from the spontaneous dynamic modelling with those obtained through our procedure adopting two smoothed slip velocity functions as input boundary condition of the elastodynamic equation on the fault plane. In other words, we use in our calculations two differently smoothed versions of the original target slip velocity function. We show the results of this comparison in Figure 6 at a specific point: panel (a) displays the temporal evolutions of the original (red line) and the two inferred (blue and green) dynamic tractions, while panel (b) illustrates the corresponding slip weakening curves. This figure demonstrates that our procedure is able to retrieve the dynamic traction evolution if the slip velocity history is relatively well known.

Despite the good agreement between the original traction temporal evolution and the two traction time histories inferred from smoothed slip velocity function (shown in Figure 6-a), Figure 6-b shows that the measure of D_c is slightly affected. The difference between the true value of D_c (0.3 m) and those estimated from the smoothed slip velocity function ($D_c \sim 0.39$ m) can be considered as an epistemic error on the estimate of D_c. Although our numerical procedure is able to constrain

reasonably well the traction evolution if slip velocity is well known, the estimate of D_c is somehow biased by a tiny difference. Indeed, any small variation on the slip velocity function (also a simple band-pass filtering) can influence the dynamic traction evolution, affecting in particular the estimate of the D_c parameter. This is in agreement with conclusions of Spudich and Guatteri (2004). It is very important to note that computations done by BIEM (Fukuyama and Madariaga, 1998) and those made by our approach based on FDM (Andrews, 1999) are identical if exactly the same slip velocity function is used. This can be considered as a useful benchmark between these two codes.

This test emphasizes the difficulty to estimate D_c by picking the end of the dynamic weakening phase from the traction versus slip curve. We automatically measure D_c for each grid point on the fault plane from the slip weakening curve using the following procedure. The traction time evolution is resampled with respect to a constant slip increment; then, the gradient of the traction as a function of slip evolution is computed and D_c value is estimated as the slip at the first positive value of the gradient being associated with the change of the traction concavity.

Figure 6-a points out that both the original "*target model*" and the inferred traction change time histories have a sharp and sudden temporal change in traction at the end of the weakening phase and a very similar duration of the breakdown phase. As expected, the weakening rate is perfectly matched. However, because slip is obtained after filtering the slip velocity time histories, the corresponding traction versus slip curves show slightly differences in the estimated D_c value (see Figure 6-b).

4. Results

In this section we present the results of our calculations to discuss the dynamic traction inferred from the kinematic models by fitting the smoothed target slip velocity time histories with the Yoffe function as described above. We compute D_c from the slip weakening curves and we compare the retrieved values with those measured from the target dynamic traction resulting from the

spontaneous dynamic simulations (see flowchart in Figure 2). We first present the results for *Model 2* (constant D_c model) and subsequently those for *Model 3* (constant D_c/D_{tot} model).

4.1 Constant D_c model (*Model 2*)

Figure 7-a shows the comparison between the original slip velocity time histories (green) resulting from the "target" dynamic model with constant D_c distribution on the fault plane, the smoothed slip velocity functions (red) and the best-fitting kinematic slip velocities (blue) retrieved by fitting the former with the Yoffe function. The 30 panels in Figure 7-a display slip velocity evolution at specific fault positions selected by taking one every five subfaults located around one of the two high slip patches (indicated by crosses in Figure 3). This figure shows that the fit to the target slip velocities through the regularized Yoffe function is quite satisfactory. Figure 7-b displays the traction time histories for the same selected subfaults, while Figure 7-c illustrates the corresponding traction versus slip curves. Despite a good agreement between slip velocity time histories, the inferred slip weakening curves depicted in panel *c* display some differences. We have verified that this difference is not caused by the adopted interpolation procedure of slip velocity time histories (see Appendix). Our results confirm that the fit to traction evolution is quite variable in space and neighbouring grid-points can display quite different slip weakening curves, also when the fit to target slip velocities is good.

This result can be explained by recalling Equation (3) and considering that dynamic traction change is determined both by the instantaneous slip velocity and by the dynamic load transferred by the neighbouring slipping subfaults. The goodness of the fit to slip velocity at most of grid-points suggests that the instantaneous contribution to dynamic traction evolution is well constrained. Because in these tests T_{acc} is imposed and equal to the real one, the positive slip acceleration and the peak slip velocity are well retrieved. However, the adopted spatial smoothing required to face the problem of the lack of physical constraints to the spatial slip velocity gradient (discussed in section

2.2) degrades the fit to traction evolution. This is particularly evident at the end of the weakening phase, thus largely affecting the estimate of D_c.

We have measured D_c from the slip weakening curves using the procedure described in the previous section. The first set of D_c values is obtained from the traction changes inferred from the smoothed target slip velocities (red curves in Figures 7 and A1), which is considered as the best representation of the original target spontaneous model. We call this model *"Model 2F"*. The second set of D_c values is retrieved from the traction changes inferred from the best-fitting Yoffe functions. We call this *"Model 2Y"*. We summarize the results of these calculations in Figure 8. Top panels display the histograms of D_c / D_{tot} ratio and of D_c values for *Model 2F* (smoothed target), while bottom panels show the histograms of D_c / D_{tot} ratio and of D_c values for *Model 2Y* (best-fitting Yoffe). We have included in Figure 8 all the subfaults having slip > 0.3 m, because this is the D_c value imposed in the spontaneous target model and to avoid measuring D_c in patches with negligible slip. D_cD_c

As expected, the inferred D_c values for the smoothed target model (see Figure 8-b) are distributed around the imposed value (0.3 m); this variability can be associated with the epistemic uncertainties in measuring D_c from slip weakening curves. Moreover, the values of the ratio D_c / D_{tot} (Figure 8-a) are distributed between 0.2 and 0.8 and this ratio is not constant for this model. This means that in this case the estimation procedure does not bias the D_c / D_{tot} ratio.

The distribution of D_c values inferred by using the best fitting Yoffe function (see Figure 8-d for *Model 2Y*) reveals the difficulties in reproducing the imposed constant value D_c and displays a larger scatter than those plotted in panel b (*Model 2F*). Finally, the distribution of the D_c / D_{tot} ratio for *Model 2Y* (Figure 8-c) displays a quite evident dispersion. Our calculations suggest that, even if D_c is not well retrieved, it does not appear any artificial correlation between D_c and D_{tot}. In other words, a poor estimate of D_c does not yield in this test a spurious correlation between values of D_c and D_{tot}.

4.2. Constant D_c/D_{tot} (*Model 3*)

Figure 9 shows the same plots presented in Figure 7 but computed for *Model 3*, the dynamic model with constant D_c/D_{tot} distribution on the fault plane. Original slip velocity time histories and dynamic tractions are shown by green curves, the smoothed target slip velocities (*Model 3F*) and the best-fitting Yoffe functions (*Model 3Y*) with their associated tractions are represented by red and blue curves, respectively. We remind that in this figure we display the grid points where we perform the fit of target slip velocity with the Yoffe function (one every five subfaults) which are located on one patch of high slip as drawn in Figure 3. The comparison between slip velocity and dynamic traction time histories as well as that between the slip weakening curves shown in this figure reveals the same features emphasized by discussing Figure 7 (see also Figure A1 in the Appendix). Thus we conclude that also in this case, even if the slip velocity history is well reproduced, the traction versus slip curves display some evident differences. These discrepancies are caused by the same effects as those discussed for *Model 2* case.

We have therefore measured D_c from the traction versus slip curves and computed the ratio D_c/D_{tot} also for *Model 3Y*. Figure 10 displays the same histograms shown in Figure 8 but computed for *Model 3*, constant D_c/D_{tot} case. Top two panels display the histograms of D_c/D_{tot} ratio and D_c values for *Model 3F*, while bottom two panels show the histograms of D_c/D_{tot} ratio and of D_c values for *Model 3Y*. For both models the inferred values of D_c/D_{tot} ratio are distributed around the value imposed (0.3) in the original target model of *Model 3* (in particular *Model 3F* is centred around 0.3 while *Model 3Y* around 0.45), while the inferred D_c values range between 0.1 and 0.6 m. The dispersion around the maximum values is symmetric in both cases, but these histograms show that the inferred D_c is biased toward high values. This systematic shift is again due to the filtering effect similar to what observed in Figure 8 for *Model 2*.

In order to provide a synoptic picture of the results of this test, we have plotted in Figure 11 the D_c distribution on the fault plane for *Model 3F* (upper plot) and *Model 3Y* (lower plot). The general pattern is similar and confirms the expected heterogeneous distribution. This figure points out that

in a model in which D_c scales linearly with final slip (D_c/D_{tot} constant) the ratio between slip weakening distance and final slip can be constrained with a reasonable uncertainty and the general spatial pattern of D_c is also reasonably imaged. This is true especially for the region where slip is large (> 0.3m, see Figure 3).

We have performed another test using the same kinematic model and the Yoffe function, but inverting simultaneously all the three parameters (T_{acc}, D_{tot} and τ_R^{eff}) characterizing the adopted source time function. In other words, instead of fixing T_{acc} to be equal to the real value of the target model, we have obtained this parameter by matching the target slip velocity as done for the other two parameters. However, the results of this further test do not change substantially with those displayed in Figures 8 and 10. This because the applied inversion procedure is able to well constrain T_{acc} and yields similar traction evolution curves to those obtained for the constant D_c / D_{tot} model.

4.3. D_c estimates with imposed constant acceleration time and slip duration

In previous sections we have presented and discussed the results of imaging dynamic traction evolution using a slip velocity time history in which the parameter T_{acc} is known a priori (that is, T_{acc} is taken equal to the true value of the target model) and the rise time τ_R^{eff} is inverted as well as those in which they are both constrained by matching slip velocity through a Yoffe function. Here, we aim to discuss the effects on the inferred traction evolution of source time functions having less constrained parameters. To this goal, we perform a test in which we use uniform constant values for both T_{acc} and τ_R^{eff} imposed a priori and not constrained by the real values of the target model. This situation is more realistic than those discussed before and quite common in kinematic modelling of earthquake source. Indeed, in practical applications the rise time (τ_R^{eff}) is not well constrained by waveform inversion approaches, while T_{acc} is unconstrained being imposed by assuming the analytical form of the source time function. For instance, a box-car function would imply $T_{acc} = 0$, while a cosine-type function (see Piatanesi et al., 2004) implies T_{acc} to be equal to half of the rise time.

In this test, we use the spontaneous dynamic model with constant D_c distribution (*Model 2*) as "target" model. The slip and the rupture time distributions are those of the "target" model, but we assume a constant rise time equal to 2.6 s and constant T_{acc} equal to 0.38 s on the fault plane. We use the inferred rupture history as a boundary condition on the fault plane and we obtain the dynamic traction evolution. We measure D_c from the slip weakening curves at each point on the fault plane. We call this model *"Model 2T"*.

We have plotted in Figure 12 the histogram of the values of D_c/D_{tot} obtained with this synthetic test for all the subfaults. This figure shows that, although D_c should not scale with D_{tot}, the inferred ratio D_c/D_{tot} is quite constant and ranges between 0.4 and 0.5. In other words, despite in the target model D_c is constant and D_c/D_{tot} is variable, we obtained an evident artificial correlation between D_c and final slip by imposing inappropriate constraints. The choice of unconstrained (wrong) values for two parameters (τ_R^{eff} and T_{acc}) characterizing the slip velocity time histories strongly affects the corresponding traction evolution as well as the retrieved slip weakening curves and hence influences the estimated D_c values.

Our results confirm the empirical relation found by Tinti et al. (2005b) between the kinematic parameters T_{acc} τ_R^{eff} and D_{tot} and the dynamic parameter D_c. In fact, according to equation (11) of Tinti et al. (2005b),

$$\frac{D_c}{D_{tot}} \propto \sqrt{\frac{T_{acc}}{\tau_R^{eff} - 1.57 T_{acc}}} \tag{4}$$

and using the values adopted in this test, we get a value of D_c/D_{tot} ~0.4, corresponding to the peak of the histogram plotted in Figure 12. Therefore, the ratio D_c/D_{tot} is totally controlled by the "wrong" values of the parameters characterizing the temporal evolution of the source time function. The results discussed in this section clearly show that a poor knowledge about the shape of source time functions as well as its time parameters (T_{acc}, τ_R^{eff}) can bias the estimate of D_c yielding spurious and artificial correlations between D_c and D_{tot}.

5. Estimates of Breakdown work

Tinti et al. (2005a) defined the breakdown work as an alternative measure of seismological fracture energy (Cocco and Tinti, 2008) to be used to characterize traction evolution curves derived from kinematic models of real earthquakes. These authors consider the possibility that traction-change and slip-velocity vectors might not be collinear, generalizing the scalar equations commonly used to estimate fracture energy. Tinti et al. (2005a) defined the breakdown work (W_b) as the excess of work over the minimum traction level ($\vec{\tau}_{min}$) achieved during slip:

$$W_b = \int_0^{t_b} \left(\vec{\tau}(t) - \vec{\tau}_{min} \right) \cdot \Delta \vec{u}(t) dt$$

(5)

where $\Delta\vec{u}(t)$ is slip velocity and $\vec{\tau}(t)$ is shear traction; t_b is the time at which the minimum traction $\vec{\tau}_{min}$ is reached at the target point (which we consider an estimate of the breakdown time $t_b \approx T_b$). W_b is an energy density (J/m^2), but Tinti et al. (2005a) called it breakdown work for simplicity.

We have computed the breakdown work for the two smoothed target models with constant D_c and constant D_c/D_{tot} at each point of the fault plane. We have plotted in Figure 13 the distribution of W_b on the fault plane for *Models 2F* (a) and *3F* (b) (upper and bottom panels, respectively). It should be noted that these distributions are not so different from the that estimated by Mikumo and Fukuyama (2006), suggesting that our numerical tests have been conducted under the condition close to the real earthquake. The average W_b values are 0.301 MJ/m^2 and 0.297 MJ/m^2 for the constant D_c and the constant D_c/D_{tot} model, respectively (i.e. models 2F and 3F). It emerges that the average breakdown work for the two target models are very similar; this is not surprising considering that the two dynamic models have similar slip and rupture time distributions on the fault plane. The average breakdown work estimated from the traction evolution curves obtained by matching the target slip velocity time histories with the Yoffe functions for both models with constant D_c and constant D_c/D_{tot} is equal to 0.315 MJ/m^2 and 0.320 MJ/m^2, respectively. These

results confirm that the breakdown work is a stable and believable parameter even if the D_c distribution is not well constrained, in agreement with the findings of Guatteri and Spudich (2000).

In order to further corroborate this result, we have compared in Figure 14 the breakdown work values estimated at each subfault from the smoothed target model (*Models 2F* and *3F*) with those estimated from the model resulting from the best-fitting Yoffe function (*Models 2Y* and *3Y*). Figure 14-a shows the comparison of breakdown work between *Models 2F* and *2Y*, while Figure 14-b displays those between *Models 3F* and *3Y*. Despite a larger scatter observed for the constant D_c model, the values inferred at each subfault by matching the slip velocity with the best fitting Yoffe function are quite in agreement with the values obtained by the smoothed target model. These results further extend the findings of Guatteri and Spudich (2000) who suggested that the fracture energy (corresponding to breakdown work in our study) is well constrained also when the estimate of other dynamic parameters (such as strength excess and dynamic stress drop) might be biased.

6. Discussion and Conclusions

The main motivation of this study is to understand the dependence of the critical slip weakening distance on the final slip during the propagation of a dynamic rupture. In particular, we are interested in understanding if the inferred correlation between D_c and final slip (D_{tot}) is a real feature of earthquake ruptures or if it arises from biases in the modelling procedures. To achieve this goal we have performed a series of numerical tests, being aware that they are not aimed at reproducing the real conditions existing in modelling observed data. On the contrary, the tests performed in this study are suitably designed to validate the adopted numerical procedure and to verify the actual capability in measuring D_c.

The results of the present study confirm that the adopted numerical procedure provides correct dynamic traction evolution when the slip history is perfectly known. However, any small modification to the real source time function affects the estimate of D_c. Indeed, we have shown in

this study that even a tiny smoothing of the slip velocity function may change the traction evolution, and hence bias the evaluation of D_c.

We have then used two spontaneous dynamic models (*Model 2*: D_c-constant and *Model 3*: D_c/D_{tot}-constant) to obtain the slip velocity and shear traction time histories that we consider as our "real target models". We have inferred the critical slip weakening distance from the imaged traction evolution curves. To this task, we have adopted a 3-D traction-at-split nodes numerical procedure (see Andrews, 1999; Tinti et al., 2005a) to retrieve the dynamic traction evolution by assuming the slip velocity history as a boundary condition on the fault plane. We have used a regularized Yoffe function (see Piatanesi et al., 2004; Tinti et al., 2005b) as source time functions in our modeling. Therefore, we have measured D_c from the slip weakening curves inferred from both the real slip velocity function of the target models (after a smoothing to reduce its high frequency content) and the best-fitting Yoffe function.

The results obtained by using *Model 2* show that we can obtain a reasonable estimate of the assumed constant D_c value only when the smoothed target slip velocity is used. Indeed, fitting the target slip velocity with a Yoffe function is not enough to retrieve the imposed D_c value. The results obtained for *Model 3* (constant D_c/D_{tot}) are slightly better. Indeed, the inferred D_c/D_{tot} ratio from both the smoothed target slip velocities and the best-fitting Yoffe functions is quite reasonably imaged, although the latter slightly overestimates the inferred D_c/D_{tot}. Nevertheless, even in this case the estimated pattern of D_c values differs from the target one. It is important to emphasize that, despite the limitations in retrieving D_c, we did not obtain any artificial or spurious correlation between D_c and D_{tot} in these tests.

Our numerical tests have shown that fitting the slip velocity functions at each point on the fault plane of the target model is not enough to retrieve good traction evolution curves and to obtain reliable measures of D_c. This is because the kinematic source models do not contain enough constraints on the gradient of slip due to both the poor resolution (both in frequency and

wavenumber) and the lack of causality constraints for dynamic rupture propagation. This is evident by looking at **Figures 7, 9 and A1**.

We have also performed a further test to mimic the common ignorance **on** the duration of the positive slip acceleration and of the whole slip velocity evolution. In fact, the kinematic models obtained from seismic waveforms usually have rather poor resolution in τ_R^{eff} and do not resolve T_{acc} at all. The results presented in this study clearly show that the poor knowledge of T_{acc} and τ_R^{eff} prevents the accurate estimation of D_c and its distribution on the fault plane. We have shown that the assumption of constant wrong T_{acc} and τ_R^{eff} introduces an artificial uniform distribution of D_c/D_{tot} on the fault plane. Large T_{acc}/τ_R^{eff} values result in larger values of D_c/D_{tot}. This means that the D_c parameter becomes a particularly large and constant fraction of total slip when particular functions, such as a triangular or a Gaussian function, are adopted as source time function in kinematic inversions. The time to peak slip velocity (T_{acc}) is one of the key parameters characterizing the earthquake source and it is directly controlled by fault constitutive properties. Simulations with spontaneous dynamic rupture models suggest that T_{acc} can change on the fault plane. This means that the use of kinematic models with a source time function incompatible with dynamic rupture simulations affects the estimate of D_c and gives an artificial correlation between D_c and D_{tot}.

Despite the difficulties in measuring D_c, our numerical tests reveal that breakdown work (as defined by Tinti et al. 2005a) is quite well constrained for both the models adopted in this study. These results represent a more general validation corroborating and extending the conclusions of Guatteri and Spudich (2000). This is particularly important because it means that seismological data can constrain breakdown work for real earthquakes. This parameter can be considered as an estimate of seismological fracture energy as discussed by Cocco and Tinti (2008).

Finally, we speculate that dynamic source models with constant slip weakening distance (D_c) should be considered unrealistic because a very heterogeneous distribution of T_{acc} and τ_R^{eff} is required on the fault plane during dynamic rupture in response to the commonly observed

heterogeneous final slip distribution. However, it should be noted that even an unphysical constant D_c model does not necessarily yield a spurious correlation with final slip. According to Tinti et al. (2005b) and to equation (4) the inferred correlation between D_c and D_{tot} is caused by the temporal evolution of slip velocity (or dynamic traction) and it is controlled by the parameters T_{acc} and τ_R^{eff}. Because these two parameters are not well constrained and they are often imposed a priori without any robust observational constraints, spurious correlations between D_c and D_{tot} can be retrieved. Moreover, we believe that the difficulties in assessing D_c by constraining the evolution of slip velocity inhibit the understanding of the physical reasons which might explain the investigated scaling. Therefore, we emphasize that constraining the slip velocity time history is a major task of future research in seismology.

Acknowledgments

APPENDIX A1

In order to check if the resulting differences between slip weakening curves of the target and the inferred dynamic models can be caused by the adopted interpolation procedure of slip velocity time history (we remind that we invert the slip velocity only at a fixed point every five subfaults), we show in Figure A1 the same plots of Figure 7 for all the sub-faults included in the box drawn in this figure.

Panel (a) in Figure A1 displays the original slip velocity time histories (green) resulting from the "target" dynamic model with constant D_c distribution on the fault plane, the smoothed slip velocity functions (red) and the best-fitting kinematic slip velocities (blue) retrieved by fitting the former with the Yoffe function. Panels (b) and (c) illustrates using the same colours the traction time histories and the corresponding slip weakening curves, respectively.

Figure A1 corroborates that the interpolation procedure does not bias the inferred traction evolution curves. Indeed, the fit to dynamic traction evolution at those grid points where slip velocity is interpolated displays a similar score to those points where slip velocity is inverted.

References

Abercrombie R., and J. R. Rice, (2005), Can obstervations of earthquake scaling constrain slip weakening?, Geophys. J. Int., 162, 406-424.

Andrews, D. J., (2002), A fault constitutive relation accounting for thermal pressurization of pore fluid, *J. Geophys. Res.,* 107, 2363, doi:10.1029/2002JB001942.

Bizzarri A., and M. Cocco, (2003), Slip-weakening behavior during the propagation of dynamic ruptures obeying rate- and state-dependent friction laws, *J. Geophys. Res.*, 108 (B8), 2373, doi: 10.1029/2002JB002198.Bizzarri A., and M. Cocco, (2006a) A thermal pressurization model for the spontaneous dynamic rupture propagation on a 3-D fault: Part I – Methodological approach, *J. Geophys. Res.,* 111, B05303, doi:10.1029/2005JB003862.

Bizzarri A., and M. Cocco, (2006b) A thermal pressurization model for the spontaneous dynamic rupture propagation on a 3-D fault: Part II – Traction evolution and dynamic parameters, *J. Geophys. Res*., 111, B05304, doi:10.1029/2005JB003864.

Bouchon, M., (1997), The state of stress on some faults of the San Andreas system as inferred from near-field strong motion data, *J. Geophys. Res.,*102(B6), 11731-1744.

Campillo M, and I.R. Ionescu, (1997), Initiation of antiplane shear instability under slip dependent friction, *J. Geophys. Res.,* 102 (B9), 20363-20371.

Chambon G., J. Shmittbuhl, and A. Corfdir (2006), Frictional response of a thick gouge sample: I Mechanical measurements and microstructures, *J. Geophys. Res.,* 111(B9) B09308, doi:10.1029/2003JB002731.

Cocco M., and A. Bizzarri, (2002), On the slip-weakening behavior of rate- and state dependent constitutive laws, *Geophys. Res. Lett., 29*, 11, doi:10.1029/2001GL013999.

Cocco, M., P. Spudich and E. Tinti, (2006) On the mechanical work absorbed on faults during earthquake rupture, in *Earthquakes Radiated Energy and the Physics of Faulting*, Eds. R. Abercrombie, A. McGarr, H. Kanamori and G. Di Toro, Geophysical Monograph Series, 170, 237-254, American Geophysical Union, Washington D. C., 10.1029/170GM24.

Cocco, M. and E. Tinti, (2008) Scale dependence in the dynamics of earthquake propagation: Evidence from seismological and geological observations, Earth Planet. Sci. Lett., 273(1-2), 123-131.

Cocco, M., Tinti, E., Marone, C. & Piatanesi, A., (2009) Scaling of slip weakening distance with final slip during dynamic earthquake rupture, in: Fault-zone Properties and Earthquake Rupture Dynamics, edited by E. Fukuyama, International Geophysics Series, 94, 163-186, Elsevier.

Dalguer L.A., Irikura K., and J. D. Riera JD, (2003) Generation of new cracks accompanied by the dynamic shear rupture propagation of the 2000 Tottori (Japan) earthquake, *Bull. Seismol. Soc. Am.*, 93 (5): 2236-2252.

Das, S., and K. Aki, (1977) A numerical study of two-dimensional spontaneous rupture propagation, *Geophys. J. Roy. astr. Soc.*, 50, 643-668.

Day, S. M., G. Yu and D. J. Wald (1998) Dynamic stress changes during earthquake rupture, *Bull. Seismol. Soc. Am.*, 88, 512-522.

Di Toro, G., D. L. Goldsby, and T.E. Tullis, (2004), Friction falls towards zero in quartz rock as slip velocity approaches seismic rates, *Nature*, 427, 436-439.

Dieterich, J. H., (1979), Modeling of rock friction - 1. Experimental results and constitutive equations *J. geophys. Res.,* 84 (B5), 2161–2168.

Dreger D., Tinti E., and A. Cirella, (2007), Slip Velocity Function Parameterization for Broadband Ground Motion Simulation, Seism. Res. Lett., 78(2), 308.

Fukuyama, E. (2003) Numerical modeling of earthquake dynamic rupture: Requirements for realistic modeling, *Bull. Earthq. Res. Inst.*, 78, 167-174.

Fukuyama, E. and R. Madariaga (1995), Integral-equation method for plane crack with arbitrary shape in 3d elastic medium, *Bull. Seismol. Soc. Am.*, 85, 614-628.

Fukuyama, E. and R. Madariaga (1998) Rupture dynamics of a planar fault in a 3D elastic medium: Rate-and slip-weakening friction, *Bull. Seismol. Soc. Am.*, 88, 1-17.

Fukuyama, E., T. Mikumo, and K. B. Olsen, (2003), Estimation of the critical slip-weakening distance: Theoretical background, *Bull. Seismol. Soc. Am.*, 93,1835-1840.

Fukuyama, E. and T. Mikumo (2004), Is Slip Weakening Distance Proportional to Final Slip?, *Seismol. Res. Lett.,* 75(2), 269 (Abstract for 2004 SSA Annual Meeting).

Guatteri, M. and P. Spudich, (2000), What can strong-motion data tell us about slip-weakening fault-friction laws?, *Bull. Seismol. Soc. Am.*, 90, 98-116.

Guatteri, M., Spudich P. And Beroza G., (2001), Inferring rate and state friction parameters from a rupture model of the 1995 Hygo-ken Nanbu (Kobe) Japan earthquake, *J. Geophys. Res.,* 106, B11, 26511-26521.

Harris, R. A. (2004) Numerical simulations of large earthquakes: dynamic rupture propagation on heterogeneous faults, *Pure Appl. Geophys.*, 161, 2171-2181.

Hillers G., Y. Ben-Zion, and P. M. Mai, (2006), Seismicity on a fault with rate- and state-dependent friction and spatial variations of the critical slip distance, *J. Geophys. Res.*, 111 (B01403), doi: 10.1029/2005JB003859.

Hirose, T. and M. Bystricky (2007) Extreme dynamic weakening of faults during dehydration by coseismic shear heating, *Geophys. Res. Lett.*, 34(14), L14311, doi:10.1029/2007GL030049.

Hirose, T., and T. Shimamoto, (2005), Slip-weakening distance of faults during frictional melting as inferred from experimental and natural pseudotachylytes, *Bull. Seismol. Soc. Am.*, 95, 1666-1673.

Ida, Y., (1972), Cohesive force across the tip of a longitudinal–shear crack and Griffith's specific surface energy. *J. Geophys. Res.* 77, 3796-3805.

Ide, S. and M. Takeo, (1997), Determination of constitutive relations of fault slip based on seismic wave analysis, *J. Geophys. Res.*, 102(B12), 27379-27391.

Lockner, D. A. and P. G. Okubo (1983) Measurements of frictional heating in granite, *J. Geophys. Res.*, 88(NB5), 4313-4320.

Ma, S., and R. J. Archuleta (2006) Radiated seismic energy based on dynamic rupture models of faulting, 111, doi:10.1029/2005JB004055.

in *Earthquakes Radiated Energy and the Physics of Faulting*, Eds. R. Abercrombie, A. McGarr, H. Kanamori and G. Di Toro, Geophysical Monograph Series,

Mase, C. and L. Smith, (1987). Effects of frictional heating on the thermal, hydrologic, and mechanical response of a fault. *J. Geophys. Res.,* 92(B7), 6249-6272.

Matsu'ura, M., H. Kataoka, and B. Shibazaki, (1992), Slip-dependent friction law and nucleation processes in earthquake rupture, *Tectonophysics,* 211, 135-148.

Mikumo, T., K. B. Olsen, E. Fukuyama and Y. Yagi, (2003), Stress-breakdown time and slip-weakening distance inferred from slip-velocity functions on earthquake faults, *Bull. Seismol. Soc. Am.*, 93(1), 264-282.

Mikumo, T., and E. Fukuyama, (2006), Near-source released energy in relation to fracture energy on earthquake faults, , *Bull. Seismol. Soc. Am.,* 96(3), 1177–1181.

Miyatake, T. (1992) Reconstruction of dynamic rupture process of an earthquake with constraints of kinematic parameters, *Geophys. Res. Lett.*, 19(4), 349–352.

Nakamura, H., and T. Miyatake (2000) An approximate expression of slip velocity time functions for simulation of near-field strong ground motion, *Zisin* (*J. Seism. Soc. Jpn.*), 53, 1-9 (in Japanese with English abstract).

Nielsen, S., and R. Madariaga, (2000), On the self-healing fracture mode, *Bull. Seismol. Soc. Am.*, 93(6), 2375-2388.

Ohnaka, M., Y. Kuwahara, and K. Yamamoto (1987) Constitutive relations between dynamic physical parameters near a tip of the propagating slip zone during stick-slip shear failure, *Tectonophysics*, 144, 109-125.

Ohnaka, M. (2003) A constitutive scaling law and a unified comprehension for frictional slip failure, shear fracture of intact rock, and earthquake rupture, *J. Geiophys. Res.*, 108(B2), 2080, doi:10.1029/2000JB000123.

Okubo, P. G. and J. Dieterich, (1984) Effect of physical fault properties on frictional instabilities produced on simulated faults, *J. Geophys. Res.*, 89(NB7), 5817-5827.

Palmer, A. C., J. R. Rice, (1973), The growth of slip surfaces in the progressive failure of over-consolidated clay. *Proc. R. Soc. London* Ser. A 332, 527-548.

Peyrat, S., K. B. Olsen, and R. Madariaga, (2001) Dynamic modeling of the 1992 Landers earthquake, *J. Geophys. Res.*, 106(B11), 26467-26482.

Piatanesi, A., E. Tinti, M. Cocco and E. Fukuyama, (2004), The dependence of traction evolution on the earthquake source time function adopted in kinematic rupture models, *Geophys. Res. Lett.*, 31, doi:10.1029/2003GL019225.

Pulido, N and K. Irikura, (2000), Estimation of dynamic rupture parameters from the radiated seismic energy and apparent stress, *Geophys. Res. Lett.*, 27(23), 3945-3948.

Rice, J. R., (2006), Heating and weakening of faults during earthquake slip, *J. Geophys. Res.*, 111, B05311, doi:10.1029/2005JB004006.

Rice, J. R., and M. Cocco, 2007, Seismic fault rheology and earthquake dynamics, in Tectonic Faults: Agents of Change on a Dynamic Earth, eds. M. R. Handy, G. Hirth and N. Hovius (Dahlem Workshop 95, Berlin, January 2005, on The Dynamics of Fault Zones), Chp. 5, pp. 99-137, The MIT Press, Cambridge, MA, USA, 446 pages.

Sen M., and P.L. Stoffa, (1991), Nonlinear one-dimensional seismic waveform inversion using simulated annealing, *Geophysics*, 56, 1624-1638.

Spudich, P., and M. Guatteri, (2004), The effect of bandwidth limitations on the inference of earthquake slip-weakening distance from seismograms, *Bull. Seismol. Soc. Am.,* 94, 2028-2036

Tinti, E., A. Bizzarri, A. Piatanesi, and M. Cocco (2004), Estimates of slip weakening distance for different dynamic rupture models, *Geophys. Res. Lett.*, 31, L02611, doi:10.1029/2003GL018811.

Tinti, E., P. Spudich, and M. Cocco, (2005a), Earthquake fracture energy inferred from kinematic rupture models on extended faults, *J. Geophys. Res.*, 110, B12303, doi: 10.1029/ 2005JB00364

Tinti, E., E. Fukuyama, A. Piatanesi and M. Cocco, (2005b), A kinematic source time function compatible with earthquake dynamics, *Bull. Seismol. Soc. Am.,* 95(4), 1211–1223.

Tsutsumi, A., and T. Shimamoto (1997), High-velocity frictional properties of gabbro, *Geophys. Res. Lett.*, 24, 699– 702.

Yasuda T., Y. Yagi, T. Mikumo, T. Miyatake (2005), A comparison between Dc'-values obtained from a dynamic rupture model and waveform inversion, *Geophys. Res. Lett.*, 32, L14316, doi:10.1029/2005GL023114

Zhang, W. T. Iwata, K. Irikura, H. Sekiguchi, and M. Bouchon, (2003), Heterogeneous distribution of the dynamic source parameters of the 1999 Chi-Chi, Taiwan, earthquake, *J. Geophys. Res.,* 108(B5), 2232, doi:10.1029/2002JB001889.
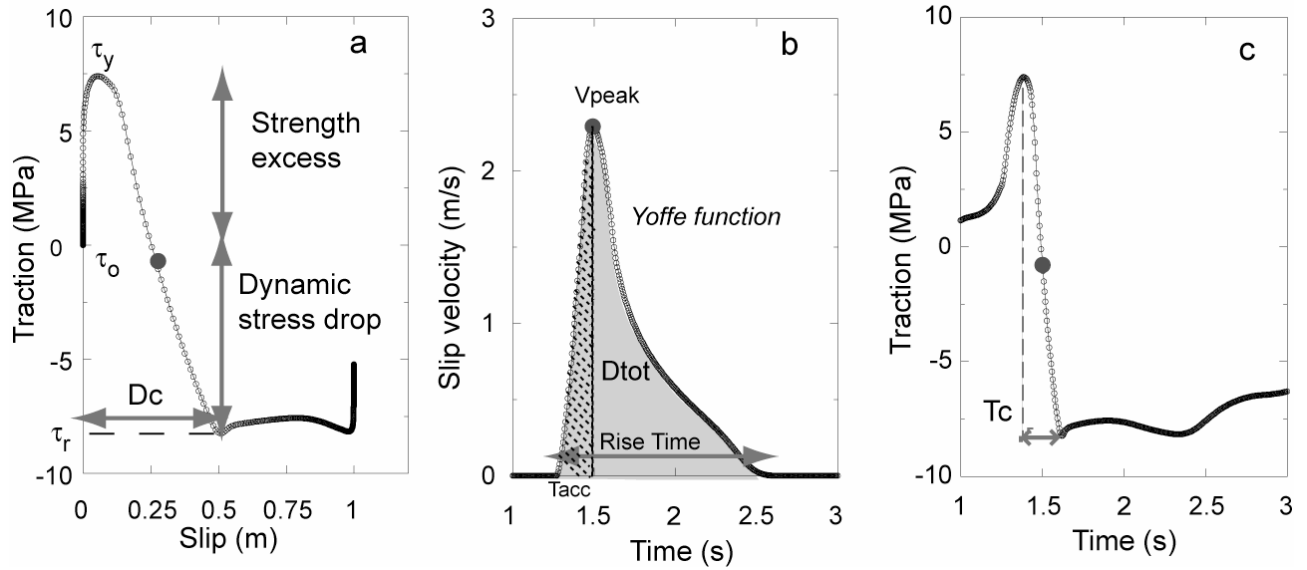
Figures:

Figure 1: Example of traction versus slip (a), slip velocity history (Yoffe function) (b) and traction history (c) for a target point on the fault plane. In each panel, the grey circle indicates the time of peak slip velocity. Different parameters are defined in the panels: dynamic stress drop, strength excess, D_c, rise time and breakdown time T_c. The shaded area in panel b indicates the final slip D_{tot} at the selected point on the fault plane. The dotted area identifies the slip velocity evolution to the peak value and its duration T_{acc}.
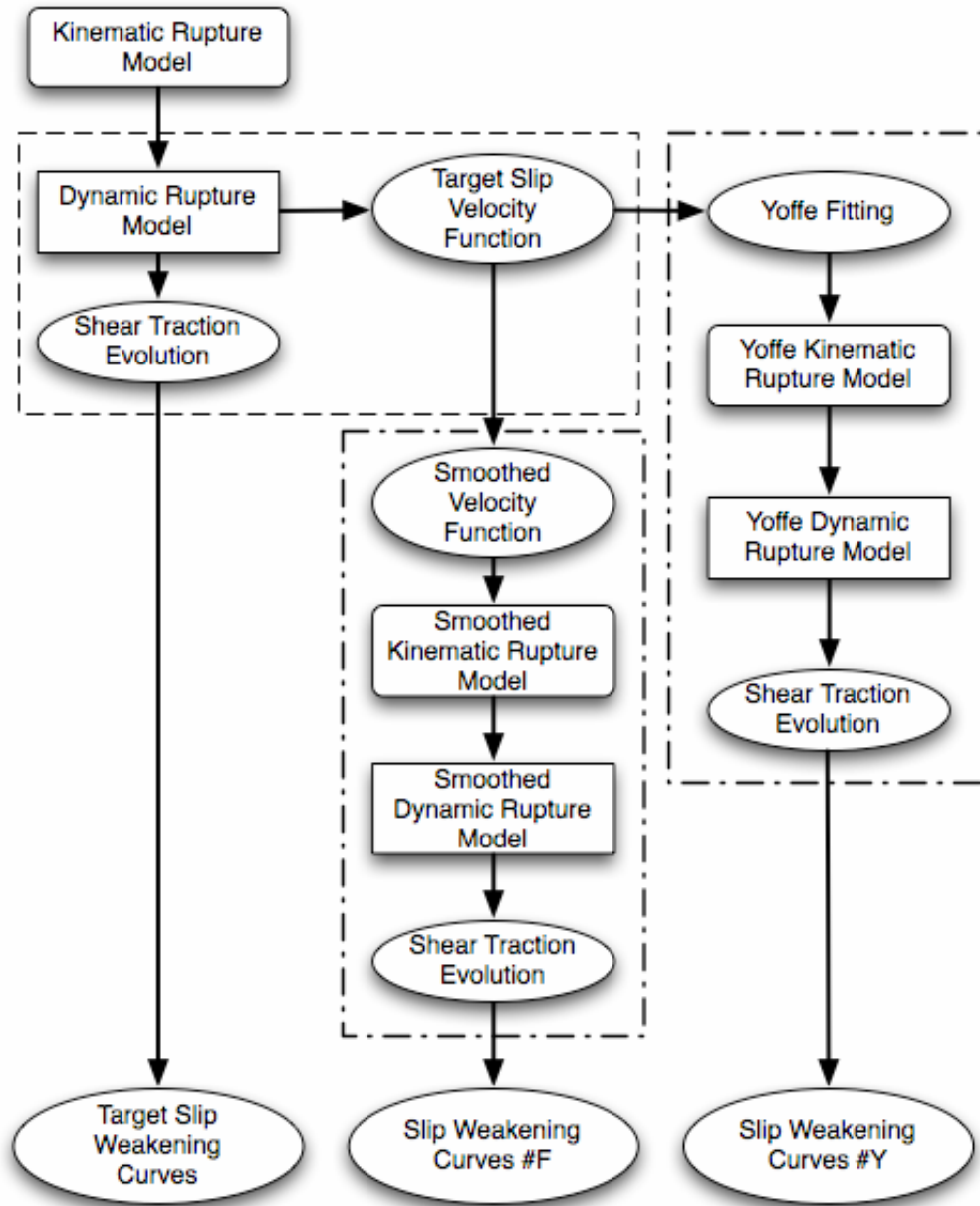
Figure 2: Flow chart of the simulation strategy adopted in this study.
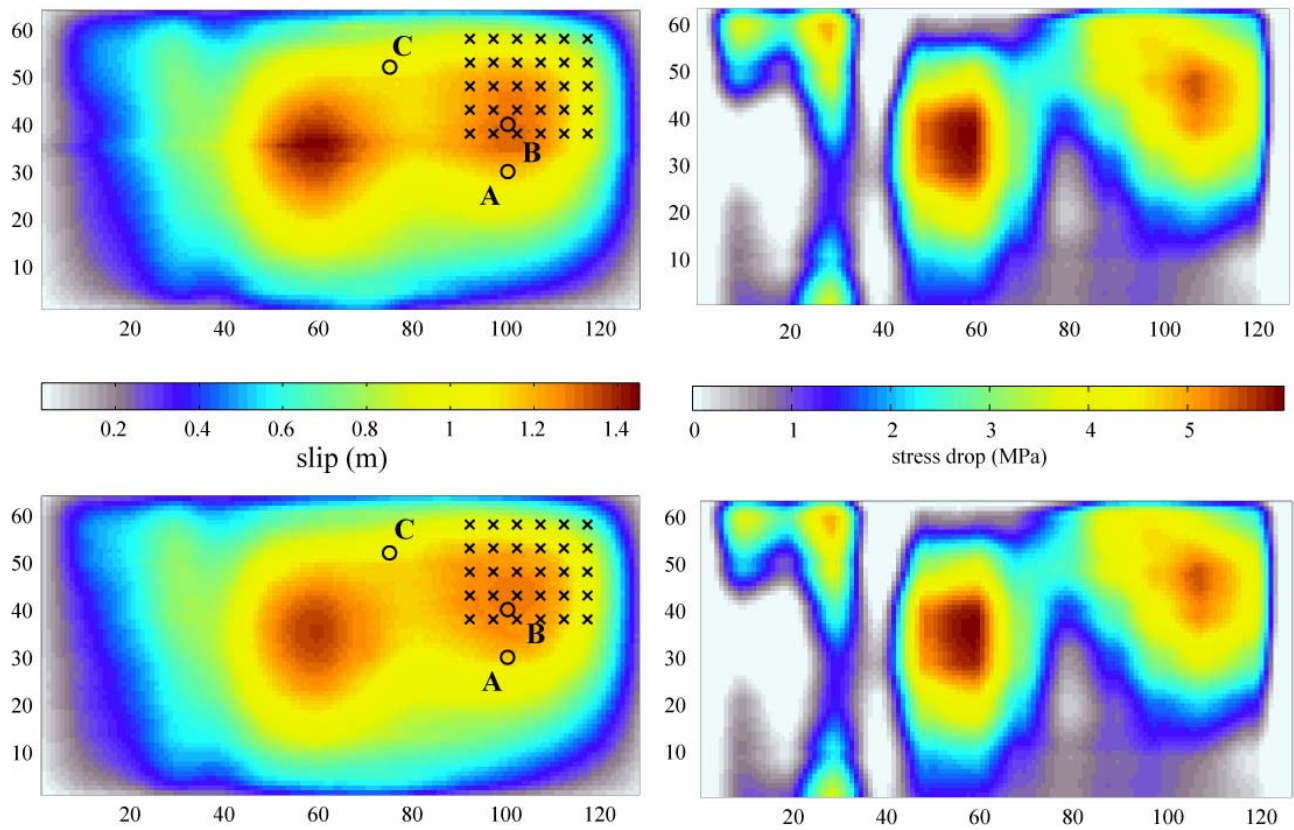
Figure 3: Slip and stress drop distributions on the fault plane for the two target dynamic models (top *Model 2* and bottom *Model 3*). Numbers along the strike and updip directions indicate the subfault number (the adopted spatial discretization is dx=200m). The fault dimension is 25.6 km along strike by 12.8 km along dip. The open circles identify the selected point to plot slip velocity and shear traction time histories shown in Figure 5.
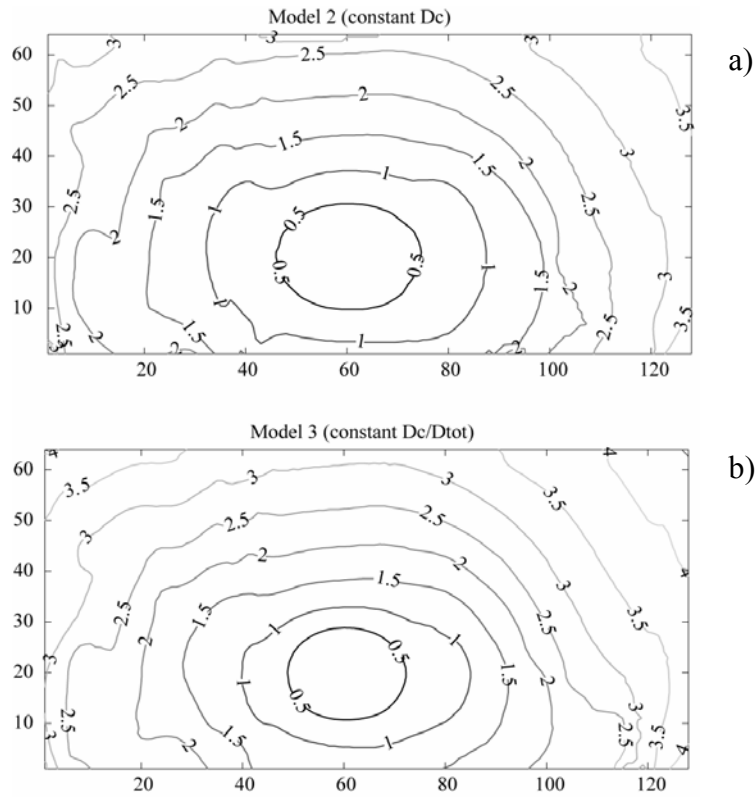
Figure 4: Rupture Time of the two target dynamic models: (a) *Model 2* (constant D_c) and (b) *Model 3* (constant D_c/D_{tot})
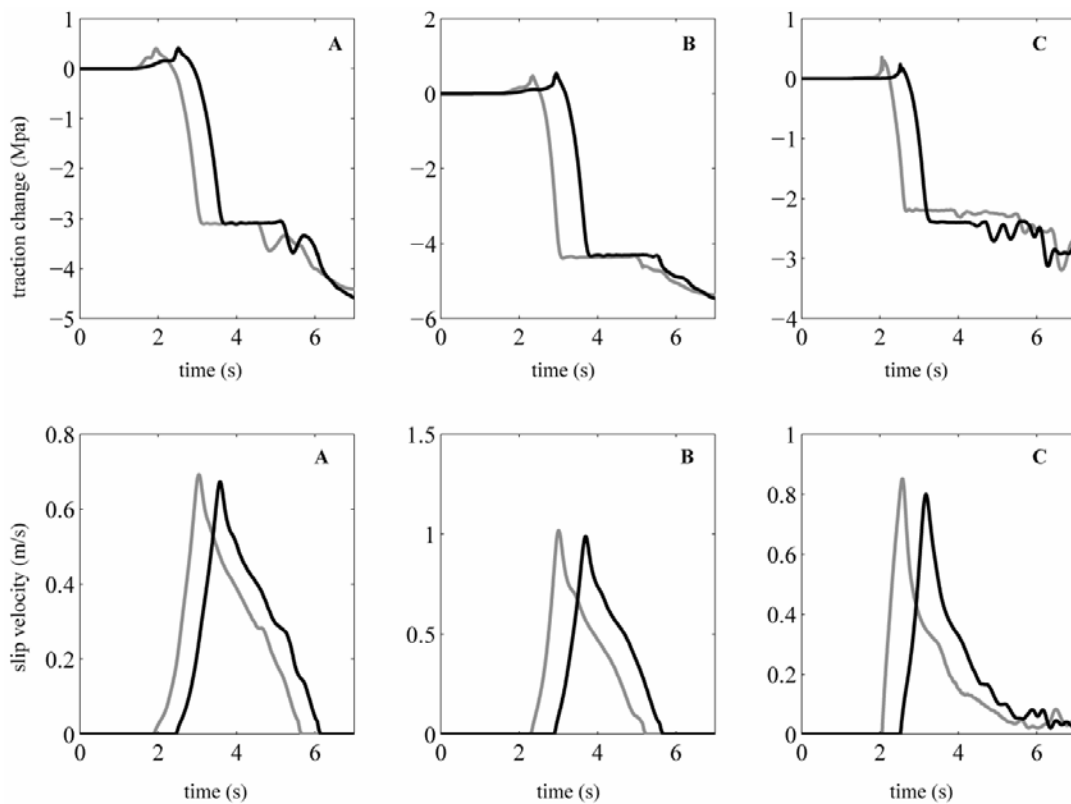
Figure 5: Traction change and slip velocity histories at three different points on the fault plane for the two models (*Model 2* and *Model 3* are grey and black, respectively). The position of target points is showed in Figure 3 as open circles.
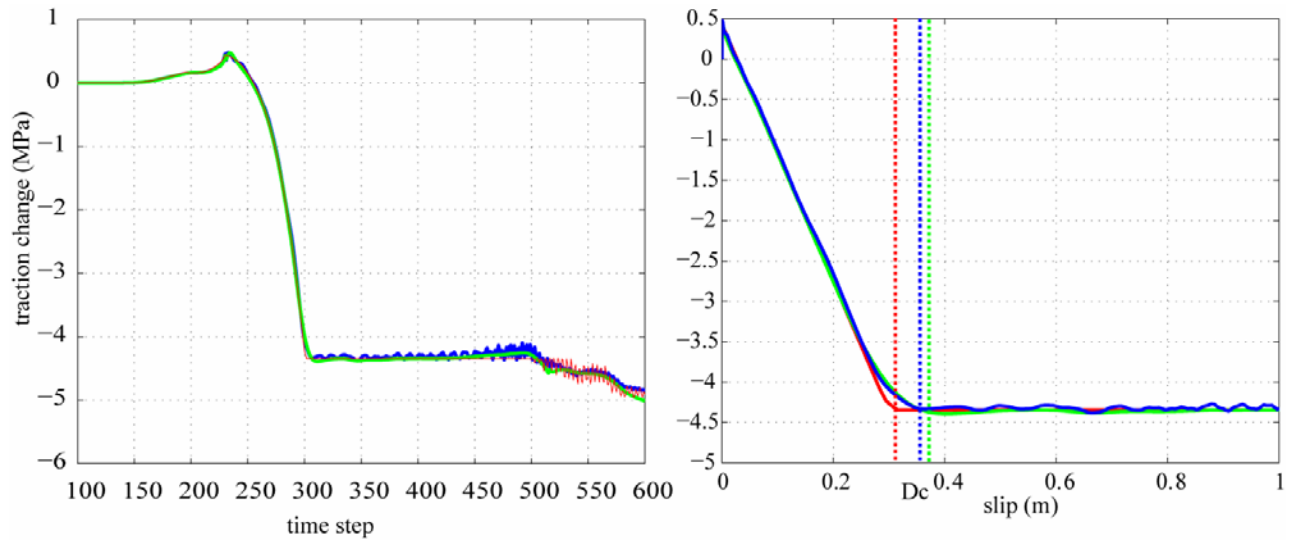
Figure 6: Comparison at a specific point of the traction time histories and traction versus slip curves for: the original dynamic model (red line), the two inferred dynamic tractions (blue and green) using two differently smoothed versions of the original target slip velocity.
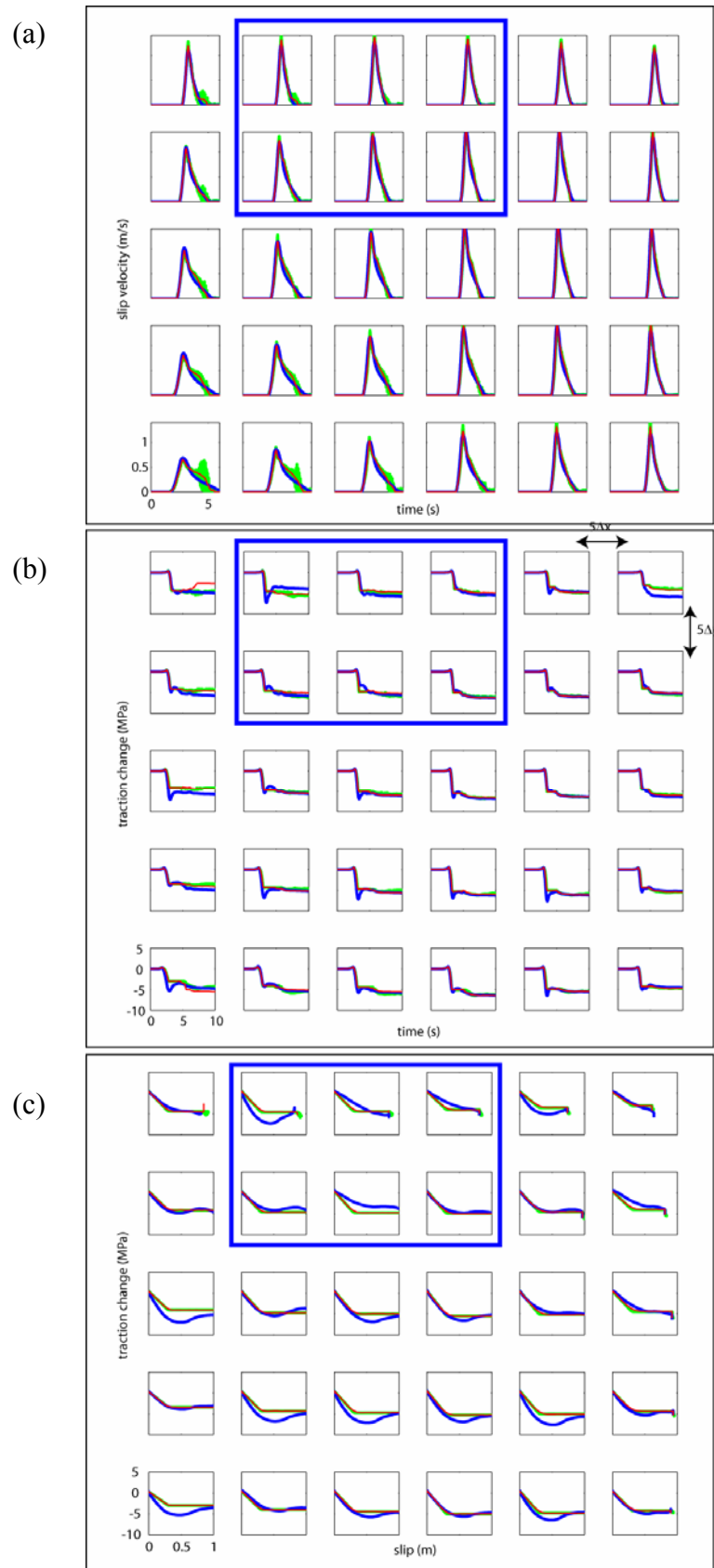
Figure 7: Slip velocity histories (a), traction histories (b) and traction versus slip curves (c) for several subfaults on the fault plane for *Model 2* (green is original target model; red is the model using smoothed slip velocity functions, blue is the model with the best-fitting

kinematic slip velocities). The subfaults positions are plotted in Figure 3 with crosses. The subfaults are selected by taking one every five subfaults.
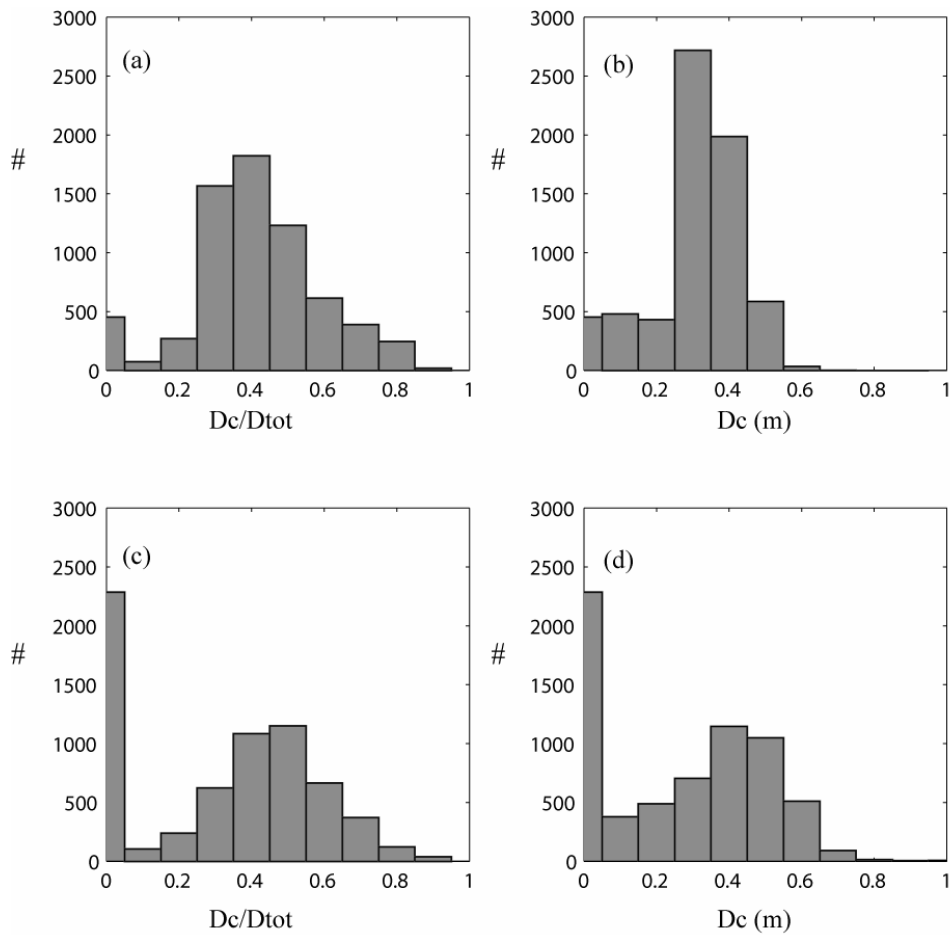
Figure 8: Result for *Model 2*. Histograms for D_c/D_{tot} (a) and D_c (b) are shown for *Model 2F*. And histograms for D_c/D_{tot} (c) and D_c (d) are shown for *Model 2Y*. In these histograms, the subfaults whose D_{tot} is less than 0.3 m are excluded. Total number of subfaults is 6684.
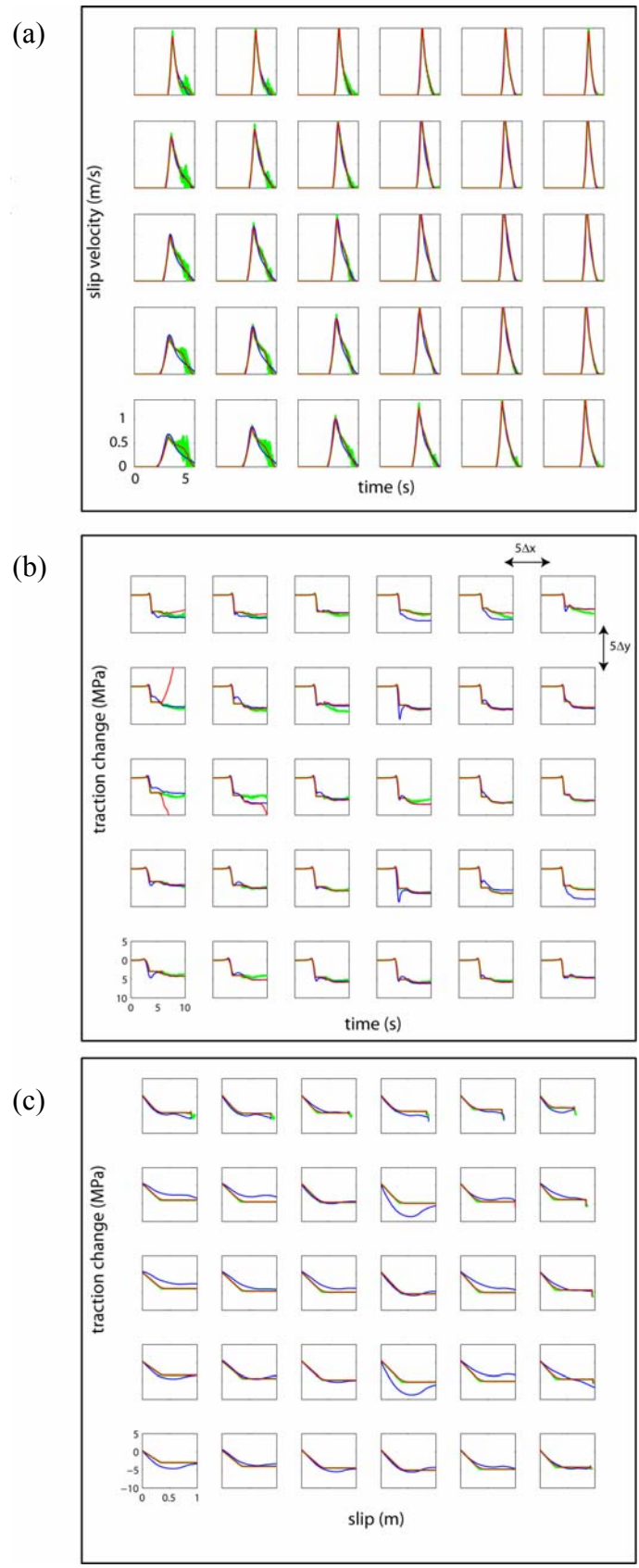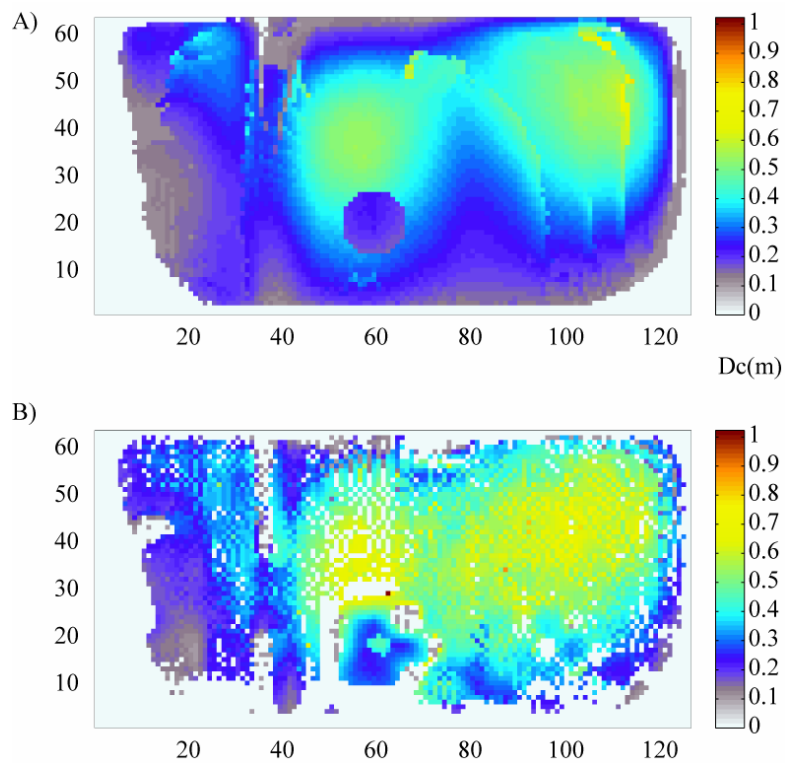
Figure 9 Same comparison as in Figure 7 for *Model 3*.
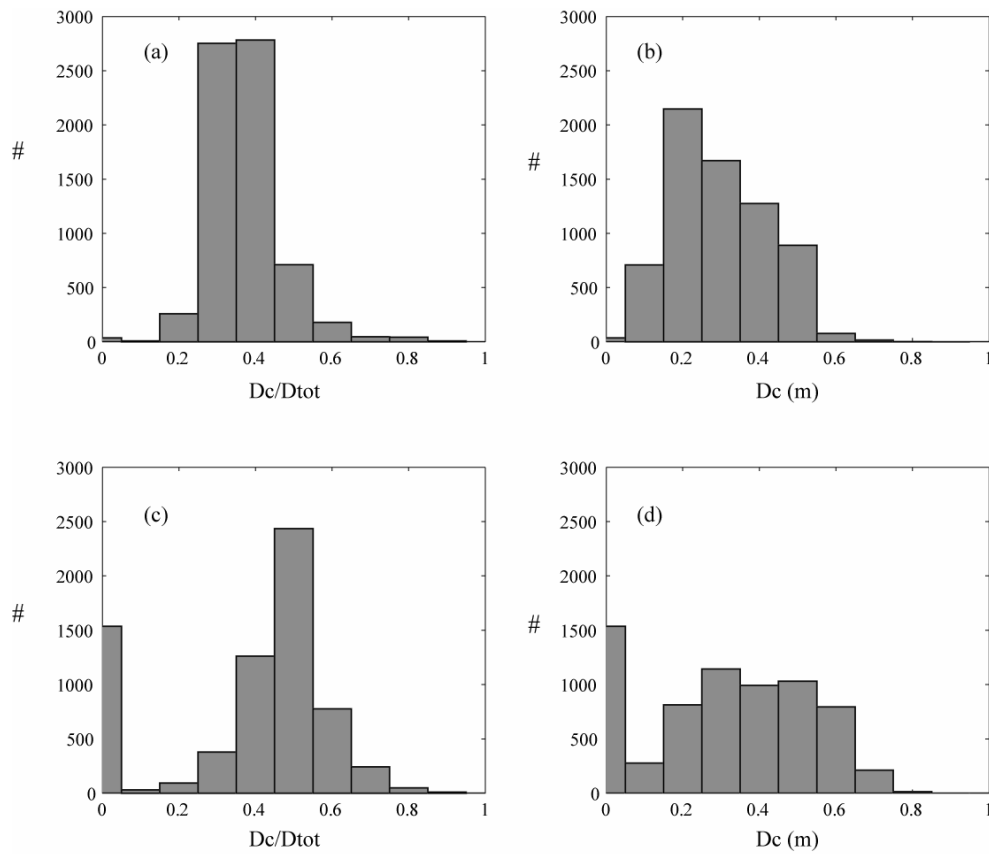
Figure 10 Result for *Model 3*. Histograms for D_c/D_{tot} (a) and D_c (b) are shown for *Model 3F*. And histograms for D_c/D_{tot} (c) and D_c (d) are shown for *Model 3Y*. In these histograms, the subfaults whose D_{tot} is less than 0.3m are excluded. Total number of subfaults is 6818.

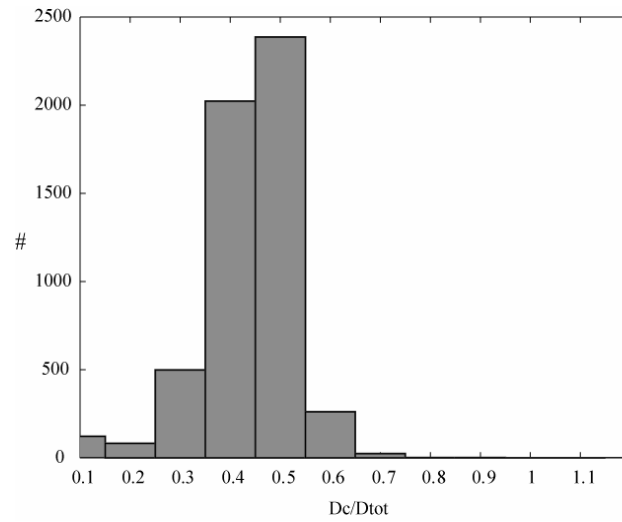**Figure 11** Distributions of D_c for *Model 3F* (a) and *Model 3Y* (b).

Figure 12 Histogram of D_c/D_{tot} for *Model 2T* (model with regularized Yoffe function assuming constant distribution on the fault plane of T_{acc} and τ_R^{eff}). D_{tot} and v_r are the same as that of *Model 2F*.
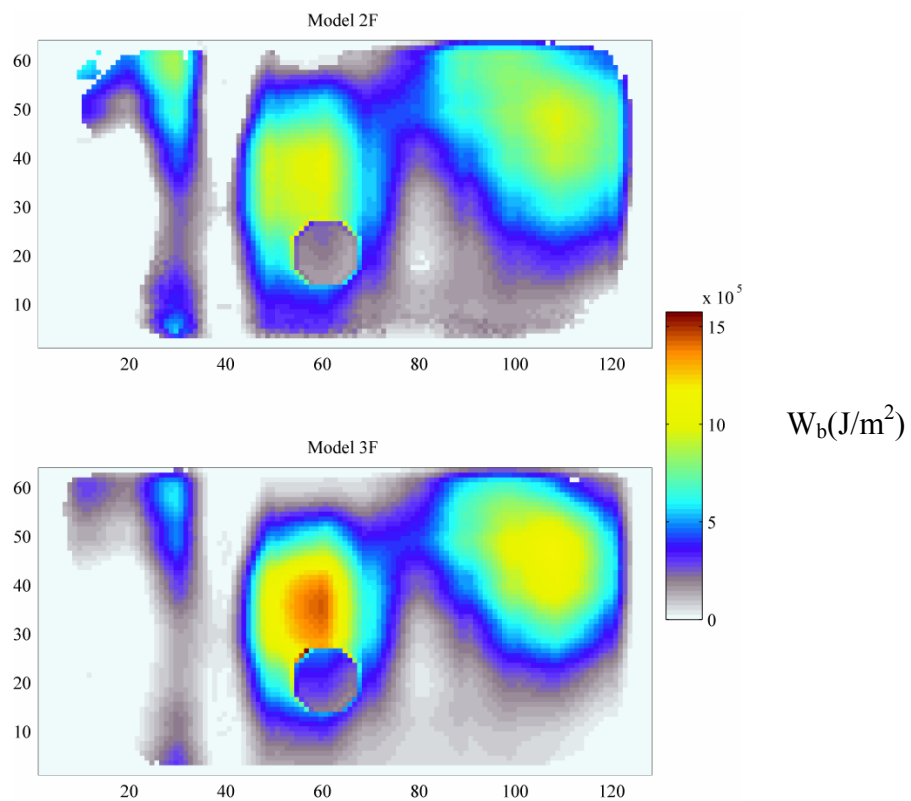

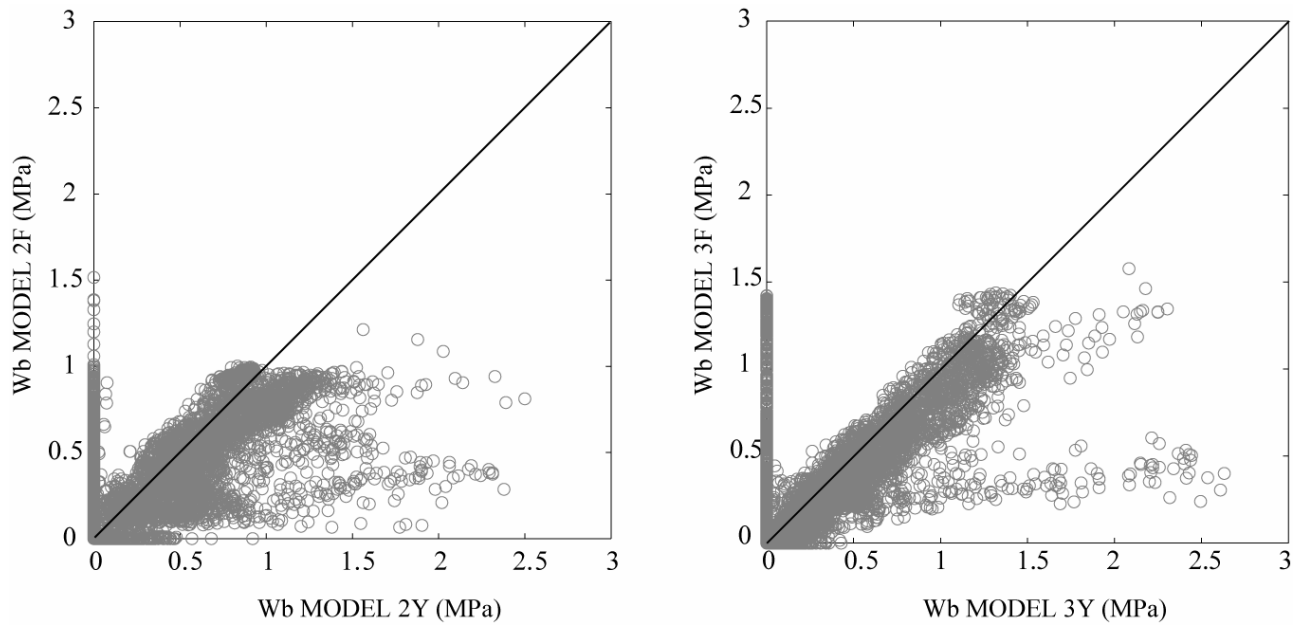**Figure 13:** Distribution of breakdown work W_b (J/m^2)for *Model 2F* (top) and *Model 3F* (bottom).

Figure 14 (a)Comparison of breakdown work W_b between *Models 2F* and *2Y* for all the subfaults on the fault plane (b) Comparison of breakdown work W_b between *Models 3F* and *3Y* for all the subfaults on the fault plane.
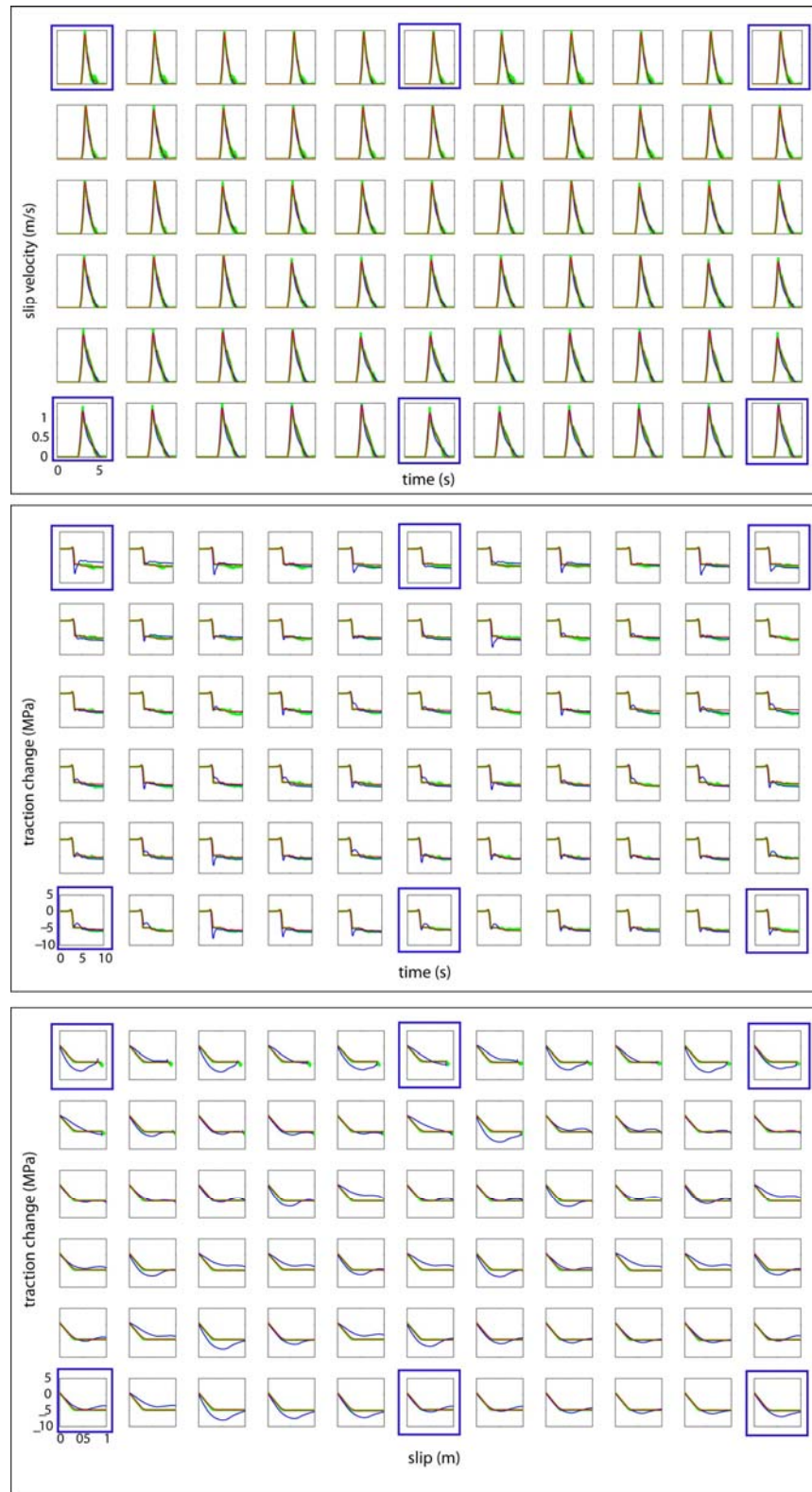
Figure A1: Same comparison as in Figure 6 for all subfaults located in the blue box of Figure 7.